RADAR OBSERVATIONS OF OCEAN SURFACE FEATURES RESULTING FROM UNDERWATER TOPOGRAPHY CHANGES

By Lisa Nyman, Björn Lund, Hans C. Graber, Roland Romeiser, and Jochen Horstmann

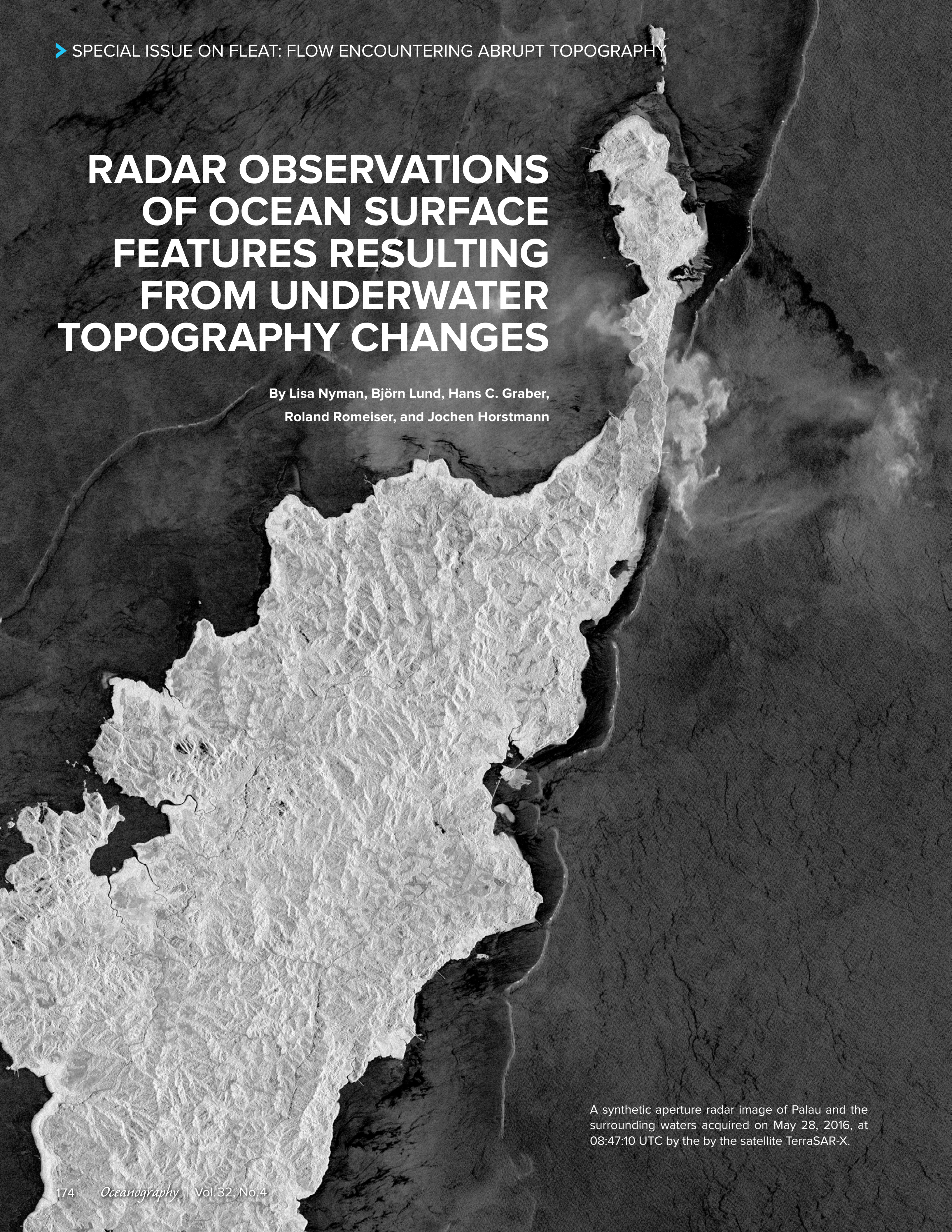

A synthetic aperture radar image of Palau and the surrounding waters acquired on May 28, 2016, at 08:47:10 UTC by the by the satellite TerraSAR-X.

> Analysis of ship-based X-band Doppler marine radar and synthetic aperture radar images ultimately enhances vessel safety in these dynamic regions.

ABSTRACT. The near-surface response to underwater topography changes is of great importance for navigational safety near regions of strong bathymetry gradients, such as around the islands of the Republic of Palau. There, mean underwater inclines can be as much as 25% of the horizontal distance, leading to a depth change of up to 85% within 26 km. Many processes associated with oceanic flows produce surface manifestations that are readily imaged from afar by synthetic aperture radar (SAR) or ship-based X-band Doppler marine radar (DMR). SAR and DMR imagery complement each other, with SAR providing a large-scale snapshot of the region on the order of 50 km or more and the DMR offering a mobile smaller-scale look at a particular area on the order of about 6 km with the ability to measure near-surface currents (1–5 m depth) in the vicinity of the ship. In this paper, we discuss the results from an analysis of thousands of DMR images around the islands of Palau. Three types of ocean surface features were identified: internal waves, surface slicks, and convergent fronts. Internal waves and convergent fronts are directly influenced by abrupt topography, and surface slicks can aid in the surface feature imaging process if their shapes are modulated by spatially varying surface currents. These ocean surface features are examined with respect to their associations with changes in the seafloor thousands of meters beneath them.

IN PLAIN WORDS. Radar imagery can provide a valuable overview of spatial characteristics of upper ocean dynamic features such as internal waves, surface slicks, and converging current fronts. Using imagery from a shipboard rotating antenna radar as well as satellite radar, we identify internal waves and their formation points as well as convergent fronts associated with abrupt bathymetry changes around Palau.

INTRODUCTION

Knowledge of abrupt underwater topography changes, as well as their effects on near-surface currents, is critical for navigational safety, search and rescue operations, and the prediction of the movements of environmental hazards such as oil slicks and other floating pollutants. Abrupt changes in seafloor topography are particularly noteworthy near the Palauan islands, with the Kyushu-Palau Ridge to the north, various seamounts in the area, and the Palau trench to the east at a depth of 8 km; the trench rapidly shoals to sea level over only 30 km horizontally (Kobayashi, 2004). It is particularly important to know the location of extreme underwater topography gradients in this region to ensure ship and submarine safety. A ship or submarine encountering an unexpected change in flow as it travels over a steep seafloor feature may be deflected off course and damaged by a collision with land, another vessel, or the topographic feature itself. In areas where the currents are not well known, remote-sensing instruments such as ship-based marine radar can help a ship's crew to identify surface currents along the ship track before they encounter a potentially dangerous region. In the region around Palau, remote-sensing instruments are an excellent choice for identifying surface features and flow changes from afar.

During a research cruise around the northern islands of the Republic of Palau from May 18 to May 28, 2016, on R/V *Roger Revelle*, the University of Miami marine radar group installed an X-band, coherent, vertically polarized Doppler marine radar (DMR) provided by Helmholtz-Zentrum Geesthacht (Figure 1a). The DMR completes one rotation every two seconds and has a range resolution of 7.5 m and an imaging radius of 3.2 km (Carrasco et al., 2017). Figure 1b shows an example DMR backscatter intensity image. The purpose of the installation was to acquire radar images for pairing with radar-derived near-surface current measurements and data from the ship-mounted multibeam echosounder. The DMR has the capability to measure near-surface currents (1–5 m depth) in the immediate area around the ship in order to determine changes in this current as the ship navigates over steep underwater topography gradients (Young et al., 1985; Senet et al., 2001; Lund et al., 2015a,b, 2018).

There are two ways to measure near-surface currents with the DMR. One is the classical dispersion shell method, which requires taking a three-dimensional Fast Fourier Transform (3DFFT) of a radar image sequence to determine the wavenumbers and associated Doppler-shifted frequencies of the surface waves resolved in the radar images. The 3DFFT method produces near-surface current maps at a resolution of ~500 m with a slightly overlapping circular grid (Lund et al., 2018). The other method to measure near-surface currents with DMR employs the Doppler velocity synthesis algorithm (DoVeS). This software was developed to measure near-surface currents around a ship with a resolution of ~326 m in non-overlapping grid boxes (Nyman et al., 2019).

The 3DFFT method is well developed and highly accurate. It compares the measured wave velocity to a theoretical wave velocity in the absence of a current, and the resulting difference is the near-surface current on which the waves travel. The 3DFFT method requires winds above 2–3 m s^{-1} and wavelengths longer than 15 m in order to work effectively. In situations where finer-scale current measurements are needed, such as at the interface of a current front or an internal wave, an alternative method for calculating near-surface currents may be used.

DMR is a coherent-on-receive radar, which means that it has the capability to measure both radar intensity and phase information. The phase information is comprehensively processed to produce Doppler velocity, which is the result of a multitude of physical processes (Braun et al., 2008; Carrasco et al., 2017). DoVeS works by synthesizing Doppler velocities from multiple look directions as the ship moves in order to determine the full Doppler velocity vector for a given region. A multiple regression analysis is carried out to empirically correct the Doppler velocity for wave contributions in order to measure a near-surface current. This analysis was trained with approximately 18,000 near-surface current measurements and compared with the shipboard acoustic Doppler current profiler (ADCP) measurements taken at 13 m depth with good results. These results can be represented in a two-dimensional, temporally averaged vector field around the ship. Alternatively, a mean for each image can be determined that will form a near-surface current transect along the ship track. Table 1 provides details of the

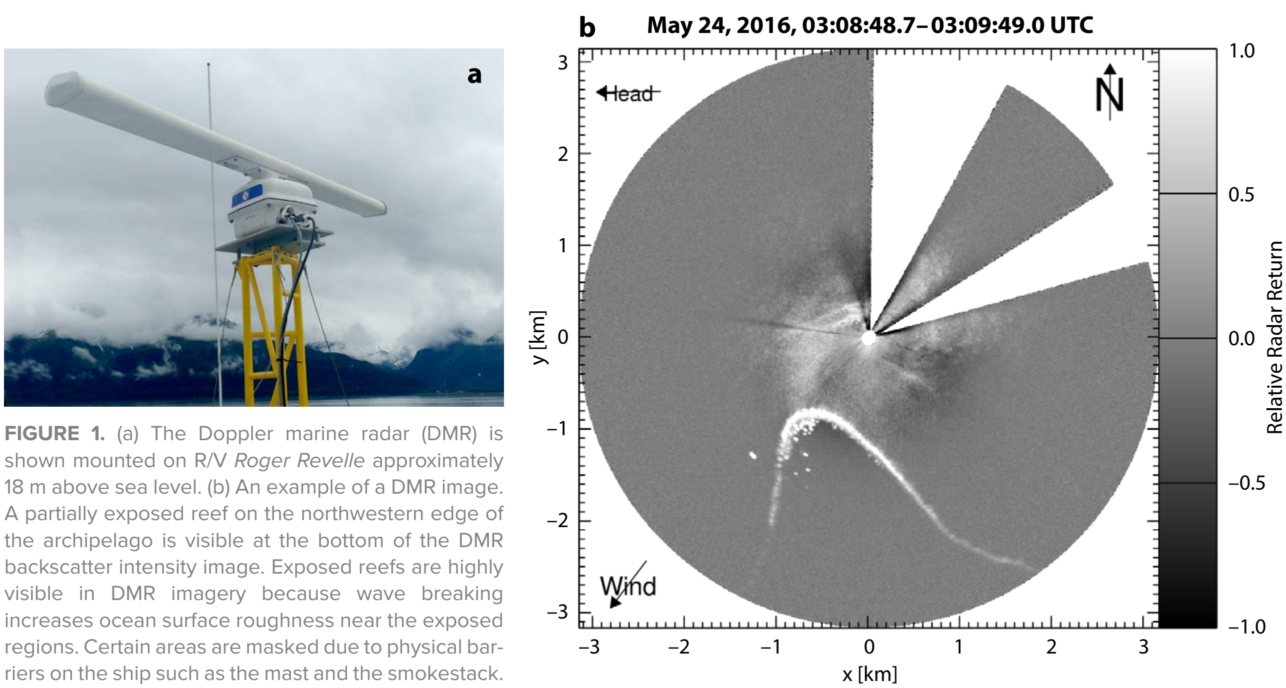

FIGURE 1. (a) The Doppler marine radar (DMR) is shown mounted on R/V *Roger Revelle* approximately 18 m above sea level. (b) An example of a DMR image. A partially exposed reef on the northwestern edge of the archipelago is visible at the bottom of the DMR backscatter intensity image. Exposed reefs are highly visible in DMR imagery because wave breaking increases ocean surface roughness near the exposed regions. Certain areas are masked due to physical barriers on the ship such as the mast and the smokestack.

TABLE 1. Sampling depth, grid type, range radius, and temporal resolution for the radar-derived near-surface current measurement methods, 3DFFT and DoVeS, used in this paper.

	3DFFT Current Field	DoVeS Current Field	DoVeS Transect
Sampling Depth	1–5 m	6–13 m	6–13 m
Grid Type	500 m diameter circles (overlapping)	326 m × 326 m boxes (not overlapping)	135 m diameter circles (overlapping)
Range Radius (distance from ship)	3.2 km	3.2 km	135 m
Temporal Resolution	10 minutes	20 minutes	75 seconds

sampling depth, grid type, range radius, and temporal resolution for the 3DFFT technique, as well as the two modes of the DoVeS technique.

During the same time period of the cruise, 34 high-resolution synthetic aperture radar (SAR) images were collected from the COSMO-SkyMed, RadarSat2, and TerraSAR-X satellites. Satellite SAR imagery provides a large-scale (50 km or more) look at the region of interest at the specific time of the satellite overpass, while the ship-mounted DMR can be taken to a region to acquire smaller-scale (6.4 km in diameter) imagery around the ship. Both SAR and DMR methods use microwave backscattering to image ocean surface roughness. To first order, the backscattered power is proportional to the intensities of the small wind-induced waves (known as Bragg waves), which have a wavelength of approximately half of the radar wavelength for radars operating at grazing incidence (Wright, 1968; Valenzuela, 1978). Therefore, in low energy wave conditions, there is reduced backscatter and thus a dark signal. In high energy wave conditions, there is increased backscatter, thus a bright signal.

In this paper, we focus primarily on radar intensity images and the signatures of marine features located near underwater topography changes measured from the shipboard multibeam echosounder around the islands of Palau. We analyze the location and orientation of these features with respect to the surrounding underwater topography and surface currents.

BATHYMETRY DETECTION WITH RADAR

It has been known since the 1980s that shallow water bathymetry can become visible in radar imagery via the modulation of surface currents. Where the water depth is shallower, the flow region is compressed, causing an amplification of the current. In deeper water, the flow region is expanded, leading to the reduction of current velocity. The region in between a faster current and a slower current (in current direction) is a convergent zone, which "squeezes" the Bragg waves to form a rough ocean surface and therefore a bright radar return is seen in these regions. In between a slower current and a faster current (in current direction), a divergent zone "stretches" the Bragg waves and results in a smoother surface and a dark radar return. Therefore, there is a dark radar return in areas of shoaling bathymetry and a bright radar return in areas of deepening bathymetry (Alpers and Hennings, 1984). Figure 2 illustrates these imaging signatures.

Figure 3 shows a SAR image containing signatures of the submerged and exposed barrier reefs off the northern coast of Babeldaob island, the largest island in the Republic of Palau. The wind conditions necessary for underwater bathymetry to be visible are that the wind speed must be above the threshold for Bragg wave generation (2–3 m s^{-1}) but below the wind speed where the wind-induced surface roughness would overpower the modulation from the bathymetry (typically 8–10 m s^{-1}). Additionally, there must be a strong current, which can be wind driven but is usually tidal, that is not running parallel to the bathymetric feature itself.

This relatively simple relationship between bathymetry and radar signatures is only expected in shallow water (typically 30 m or less), so it is not possible to determine bathymetry changes in this way at water depths greater than 30 m, where the relationship between depth and surface current is more complicated. However, in certain situations,

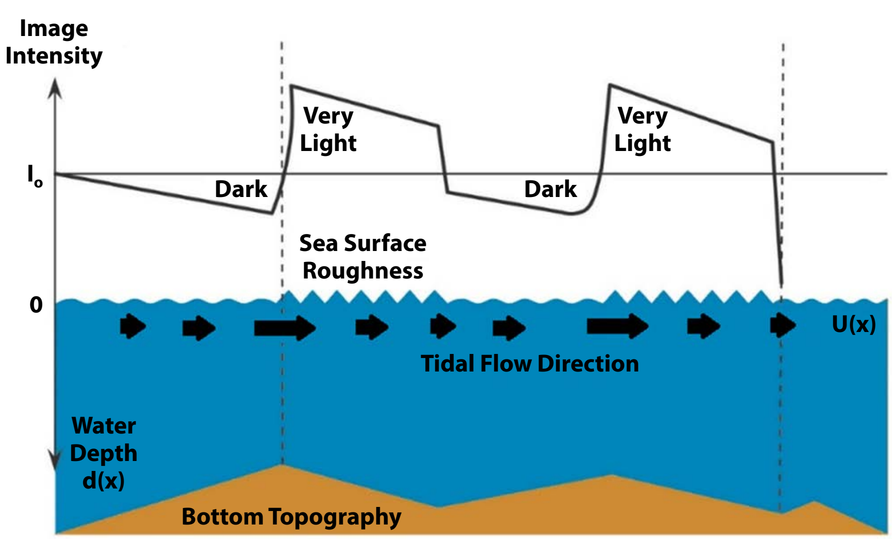

FIGURE 2. The wave-current interaction mechanism by which shallow water bathymetry is imaged with synthetic aperture radar (SAR). *Adapted from Alpers et al. (2004)*

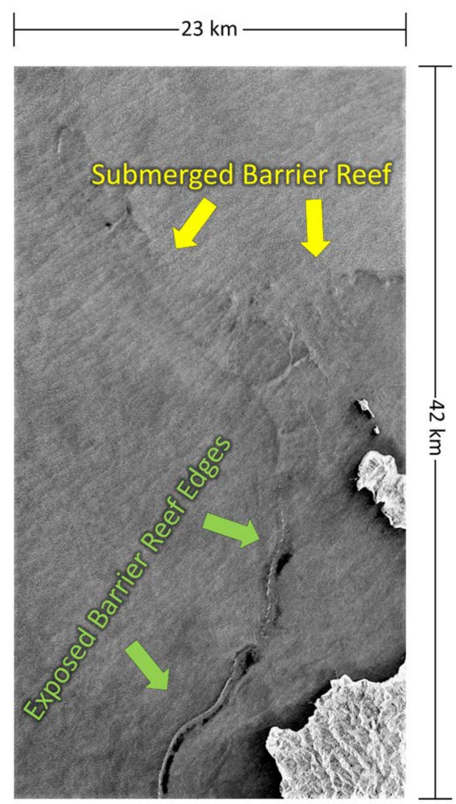

FIGURE 3. A SAR image acquired on November 6, 2015, at 08:44:00 UTC by the satellite COSMO-SkyMed, exemplifies the imaging of shallow water bathymetry of the submerged reefs around Palau.

the DMR can image features that are directly correlated with large topography changes in deep water. During the 10-day *Revelle* cruise in May 2016, the polar DMR backscatter intensity data were converted to Cartesian coordinates and averaged to images every 75 seconds, creating over 10,000 DMR average intensity images. By individually scrutinizing this large number of images, radar images with pronounced signals of oceanic features of interest were separated into three categories: internal waves, slicks, and fronts. Figure 4 shows examples of each of these signatures. Of the 10,058 images, nine contained evidence of internal waves or internal wave packets, 67 contained slicks, 12 contained convergent fronts, and 9,968 showed no notable features. In some of these images, there is more than one instance of a single type of feature or two different types of features. In subsequent images, the same feature is seen at different times as the ship travels. Six different internal waves or internal wave packets were identified, 602 separate slicks, and six convergent fronts.

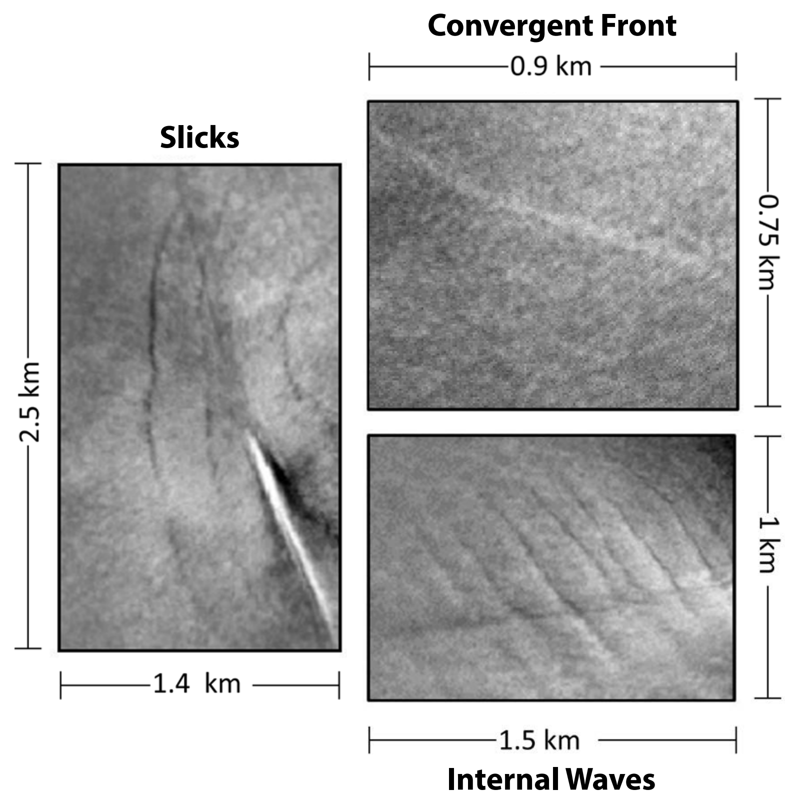

FIGURE 4. Examples of DMR images show the signatures of a surface slick, a convergent front, and an internal wave packet. Surface slick signatures are defined as dark quasi-linear features, front signatures are defined as single bright linear features, and internal wave signatures are defined as juxtaposed alternating bright and dark linear features. Logarithmic scale is from –1 to 1 dB from black to white.

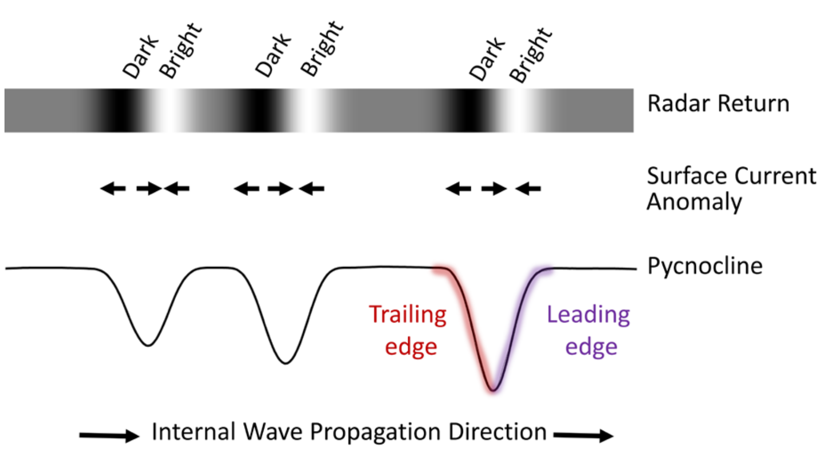

FIGURE 5. A radar imaging pattern of surface manifestations over an internal wave.

INTERNAL WAVES

Internal waves occur at the pycnocline interface of a stratified water column. They are seen in radar imagery as juxtaposed bright and dark linear or arc-shaped strips on a gray background. Internal wave signatures appear linear-shaped in DMR images (which have an imaging diameter of 6.4 km) and arc-shaped in SAR imagery (which can cover a much larger area of 50–100 km). The orbital motions within an internal wave modulate the surface current such that there is a converging current on the leading edge of the wave and a surface current divergence on the trailing edge of the wave. Thus, due to wave-current interaction, there is a bright radar return on the leading edge of an internal wave and a dark return on the trailing edge (Alpers, 1985). Figure 5 shows the alternating bright-dark radar signature pattern and the associated internal wave shape. While both internal wave signatures and signatures of changing bathymetry described in the previous section display an alternating bright-dark pattern in radar imagery, they are easily differentiated. Internal wave signatures are visible on a smaller scale with a distinct regular periodicity, with approximately 20–50 m between neighboring waves within an internal wave packet. Changing bathymetry signatures are irregularly shaped according to the local bathymetry and are visible in SAR imagery over a much larger length scale of tens of kilometers.

Internal waves commonly form as a result of stratified flow encountering a sudden underwater topography change. In a simple stratified two-layer model, shown in Figure 6, internal waves are

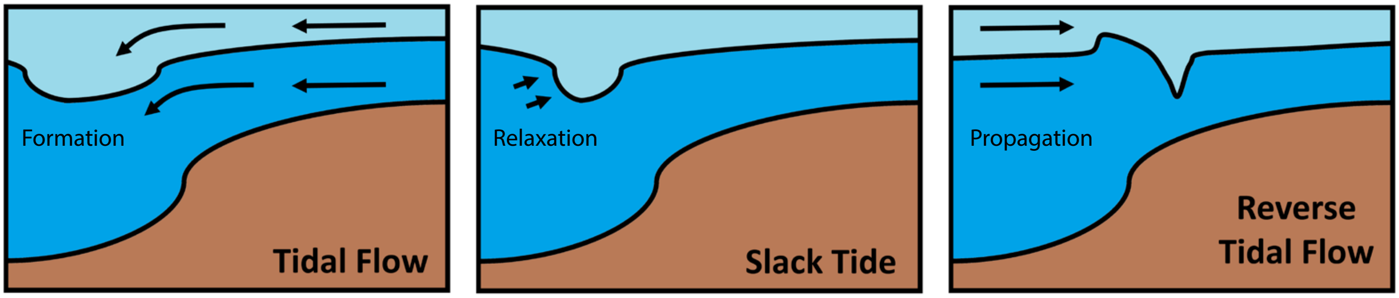

FIGURE 6. Schematic showing the formation of internal waves by a tidal current over changing bathymetry.

often formed by tidal flow depositing the upper layer of water in an indent into the lower layer that follows the shape of the bathymetric feature. During slack tide, this perturbation relaxes, creating a distinct depression in the water column. When the tide reverses, this depression propagates in the direction of the flow (Lamb, 1994). This perturbation often creates a train of internal depression waves that propagate together in a packet.

Four single internal waves and two internal wave packets were identified in DMR mean backscatter intensity images. The propagation direction was determined by their orientation. We ray traced the internal waves along a great-circle arc (the shortest possible connecting line between two points along the surface of a spherical Earth) in both directions perpendicular to the internal wave orientation. Tracing the great-circle arc 100 km in either direction and plotting it against a bathymetric map of the region, we followed the arc until it crossed a likely formation point. The most probable internal wave generation point was systematically determined by identifying the area where there is a sharp drop in bathymetry along each internal wave's great-circle arc that is not blocked by land.

From this analysis, internal wave generation points are determined (Figure 7). Internal waves B and F have likely formation points on the northern tip of Velasco Reef, a sunken coral atoll north of the inhabited Palauan islands. Velasco sits at a depth of only 15 m, (Colin, 2009) and the current is therefore directed around the reef. The fact that the great-circle arcs of internal waves B and F intersect indicates that they may be different stages of the same tidal formation. This could indicate that the internal wave forms off the northern tip of the reef and initially propagates west, but it refracts around the curvature of the atoll and then propagates in a southwest direction.

Internal wave A likely has a nearby formation point, where the northern part of Velasco meets the southern end of the Kyushu-Palau Ridge (Figure 8a). This ridge extends north 2,600 km to Japan and has been previously identified as an internal wave generation spot (Wolanski

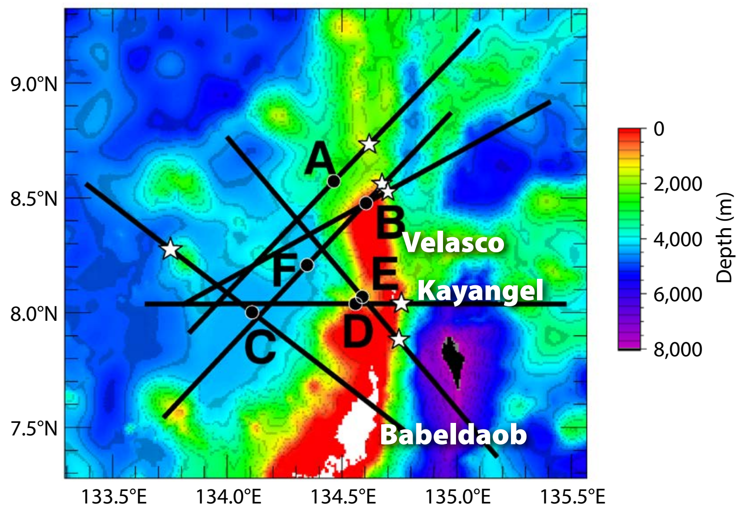

FIGURE 7. Ray tracing of the six internal waves imaged during the May 2016 cruise overlaid on a bathymetric map of the area. Black circles mark the locations where internal waves or internal wave packets were originally seen. The black lines are great-circle arcs extended 100 km in each direction perpendicular to internal wave orientation, and white stars are the locations of the most likely formation points.

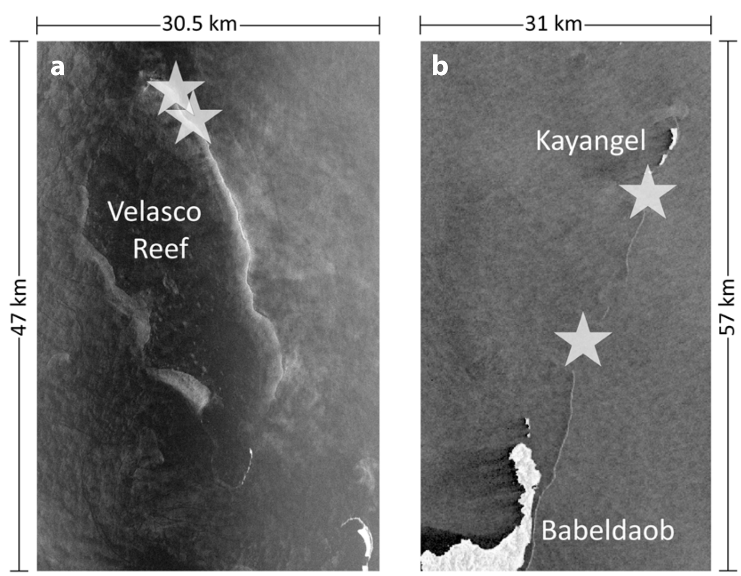

FIGURE 8. SAR images of the two primary internal wave generation regions identified by ray tracing analysis. Formation points are indicated by stars, similar to Figure 7. (a) This image of Velasco Reef was acquired by COSMO-SkyMed on May 24, 2016, at 09:07 UTC. (b) An image of the region between Kayangel and Babeldaob was acquired by the TerraSAR-X satellite on May 23, 2016, at 08:38 UTC.

et al., 2004). Internal waves E and D have formation points near the narrow waterways between the island of Kayangel and reefs north of Babeldaob (Figure 8b). The narrow opening between the reefs paired with an abrupt ridge is the perfect internal wave formation scenario. Internal wave C has a most likely formation point at the small seamount west of the main archipelago.

SLICKS

Marine features categorized as surface films ("sea slicks") are ubiquitous in the area around Palau, where they typically have a continuous linear shape. Because they dampen the Bragg waves and thus appear as smooth water (Hühnerfuss and Alpers, 1983), sea slicks manifest as areas of low backscatter (dark returns) on the radar. These features can be biological films or man-made slicks such as oil spills (Hovland et al., 1994). In the tropical waters around Palau, biogenic films commonly result from life processes of local phytoplankton and zooplankton. In the presence of convergent ocean currents, slicks align within a convergent zone (da Silva et al., 1998). They are advected by the surface current, and their irregular shapes in radar images can act as tracers for physical processes (Gade et al., 2013). Figure 9 depicts sea slicks in both DMR and SAR images of the area. The wide distribution of slicks throughout the region indicates that these dark features are not directly correlated with topography changes. However, the traces slicks leave on the ocean surface aid in the imaging of flow patterns that may distort the slick.

For example, in Figure 9b, the slick is altered by an internal wave packet that formed near the northern barrier reef off Babeldaob Island. This slick is most likely biogenic because it is so close to the productive coral reefs around the island. The presence of this slick aids in the imaging of the internal wave packet. The zigzag slick pattern in Figure 9b is seen only once out of 602 incidences of slicks we imaged during the cruise. The periodic alternating bright-dark signature in the image indicates the presence of an internal wave, which is packet E in Figure 7. The patterns produced from the slick's distortion suggest that the alternating surface current within the internal wave packet is advecting the slick in an interchanging motion. The angle between the slick orientation and the internal wave propagation direction alters its shape. In regions of convergence, the slick is pulled to the northeast, whereas in divergent regions, the slick is pulled to the southwest, creating a discontinuity that allows the feature to be identified more clearly.

CONVERGENT FRONTS

During the 10-day cruise, continuous radar operation revealed only six high backscatter areas attributed to convergent fronts, all of which occurred over abrupt underwater topography changes. The radar signature of a convergent front is defined as a thin strip of uniformly rough water on either side of the topographic feature that is associated with a converging current shear. Wave-current interaction along the converging current shear interface produces the surface signature seen in radar (Lyzenga, 1991). A unique quality of the convergent fronts seen in the DMR images around Palau is that they are only visible in temporally averaged images. In single rotation images, convergent fronts are invisible, because wave motions eclipse the relatively weak bright radar signature. Because of this, these types of fronts are also not observed in the SAR images of the area, which display a snapshot of the area taken in less than a second. In the DMR mean intensity images, many waves will average out

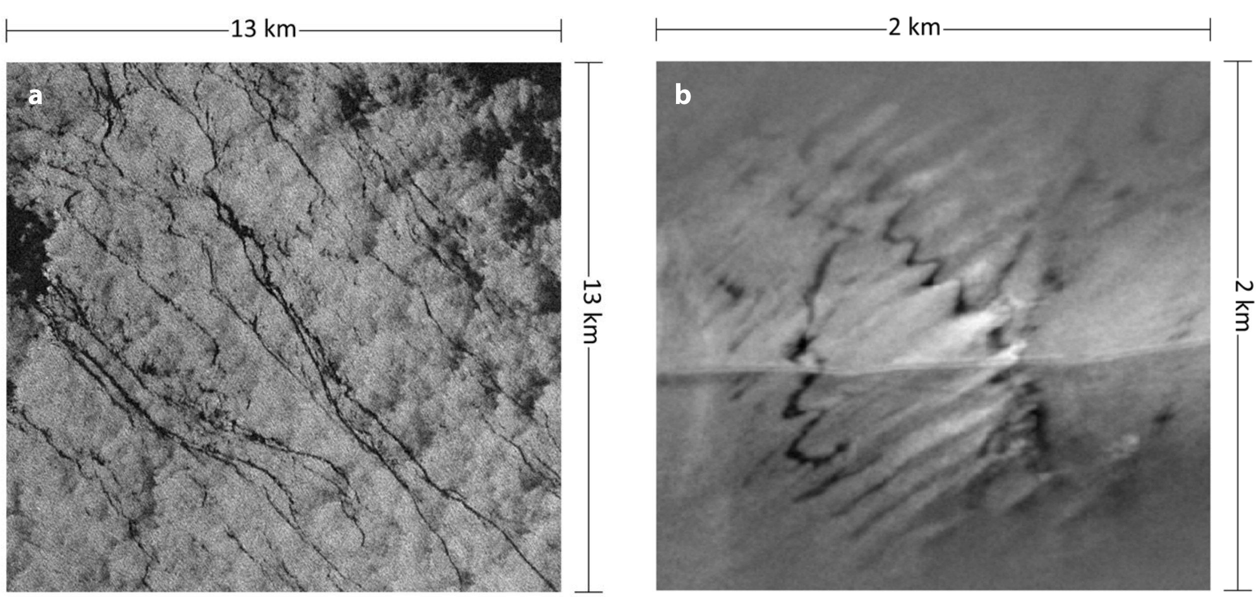

FIGURE 9. (a) A subscene of a COSMO-SkyMed image acquired on June 14, 2016, at 08:42 UTC shows surface slicks near Palau. (b) Surface slicks advected by the internal wave motions can be identified in this temporally averaged DMR image acquired on May 27, 2016, from 08:11 to 08:20 UTC. The horizontal line in the middle is the ship wake.

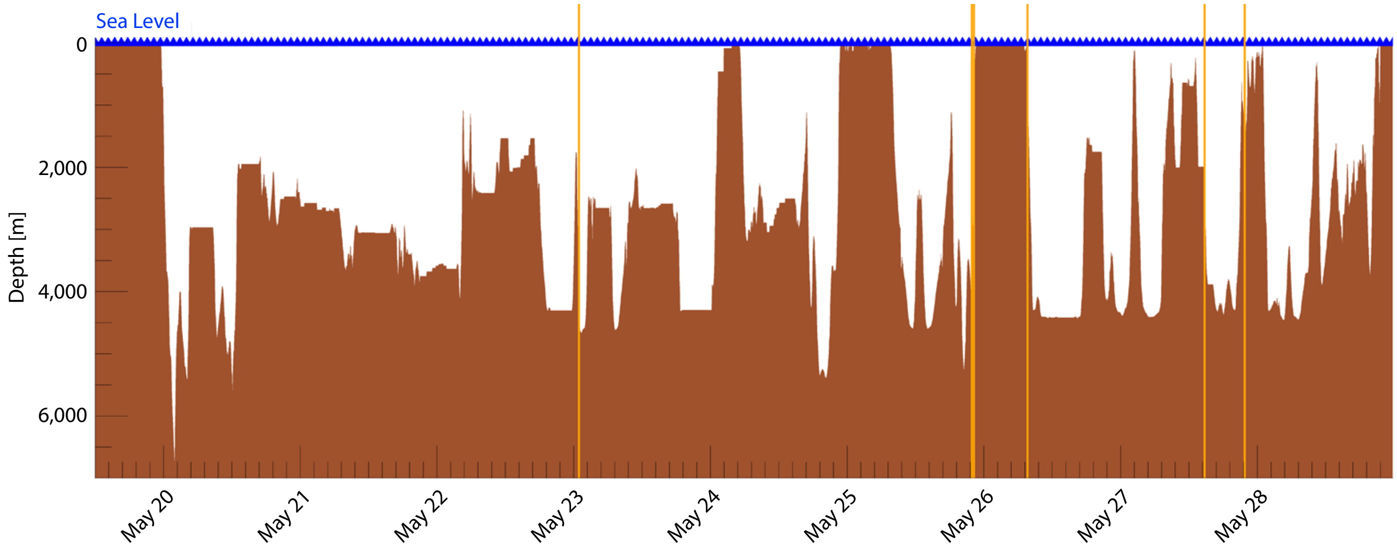

FIGURE 10. A time series of the underwater topography beneath the ship track compared with the times of frontal feature sightings represented by orange bars.

over time to a uniform background, and the convergent fronts appear as bright lines that can be faint or bold, depending on the strength of the convergence. All of the identified front signatures on this cruise were distributed near abrupt changes in underwater topography.

Over the course of the cruise, six convergent front signatures were documented. All of them are visible in wind speeds between 3 m s^{-1} and 8 m s^{-1}, and all are associated with abrupt underwater topography changes greater than 1,500 m over a relatively short horizontal distance. In Figure 10, a time series of the underwater topography beneath the ship track is compared to times of front signature sightings, represented by orange vertical lines. While a convergent front does not always occur when currents encounter abrupt underwater topography, convergent front signatures that do occur are consistently associated with sudden underwater topography changes.

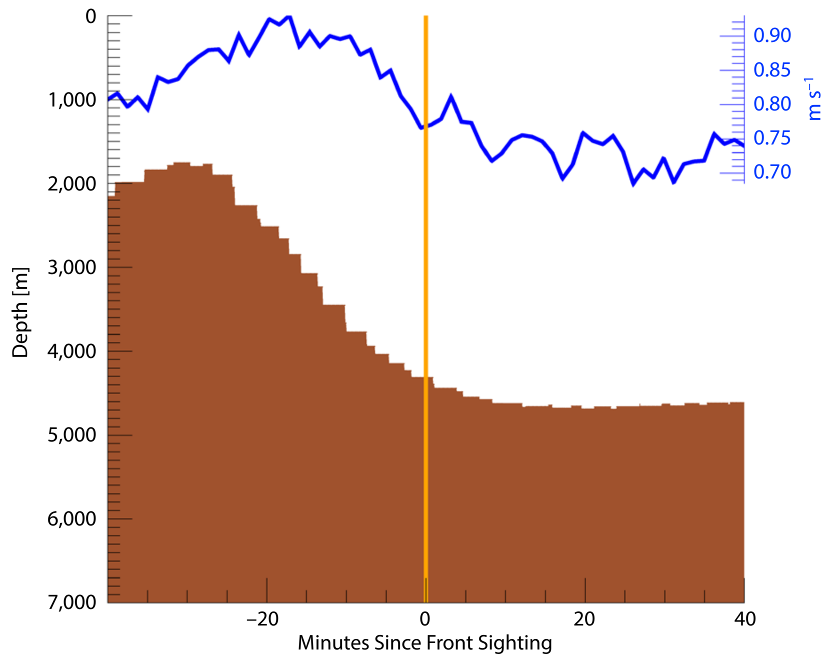

FIGURE 11. The bathymetry under the ship track compared with the DoVeS current magnitude 40 minutes before and after the convergent front sighting.

On May 23, 2016, when the first convergent front signature of the cruise was observed, near-surface currents close to the ship were extracted from the data with the DoVeS algorithm. In Figure 11, a transect of the magnitude of DoVeS-derived near-surface currents close to the ship is overlaid on the underwater topography beneath the ship track 40 minutes before and after the front sighting. The near-surface current for this time period is directionally steady at about 261° from north. The ship is also traveling steadily in a similar direction 226° from north. The magnitude transect shows that the current decreases by about 20 cm s^{-1} as the bathymetry drops approximately 2,000 m over an 18 km horizontal distance, creating sufficient convergence for the front interface to be visible.

A bright front signature is not always caused by increasing or decreasing upper ocean currents. Often, a near-surface directional current change creates a strong convergence along its interface. This is the case on May 27, 2016, 14:50 UTC, and May 27, 2016, 21:14 UTC, when the wind speed was greater than 3 m s^{-1}, and thus the sea state was high enough to obtain reliable two-dimensional dispersion shell cur-

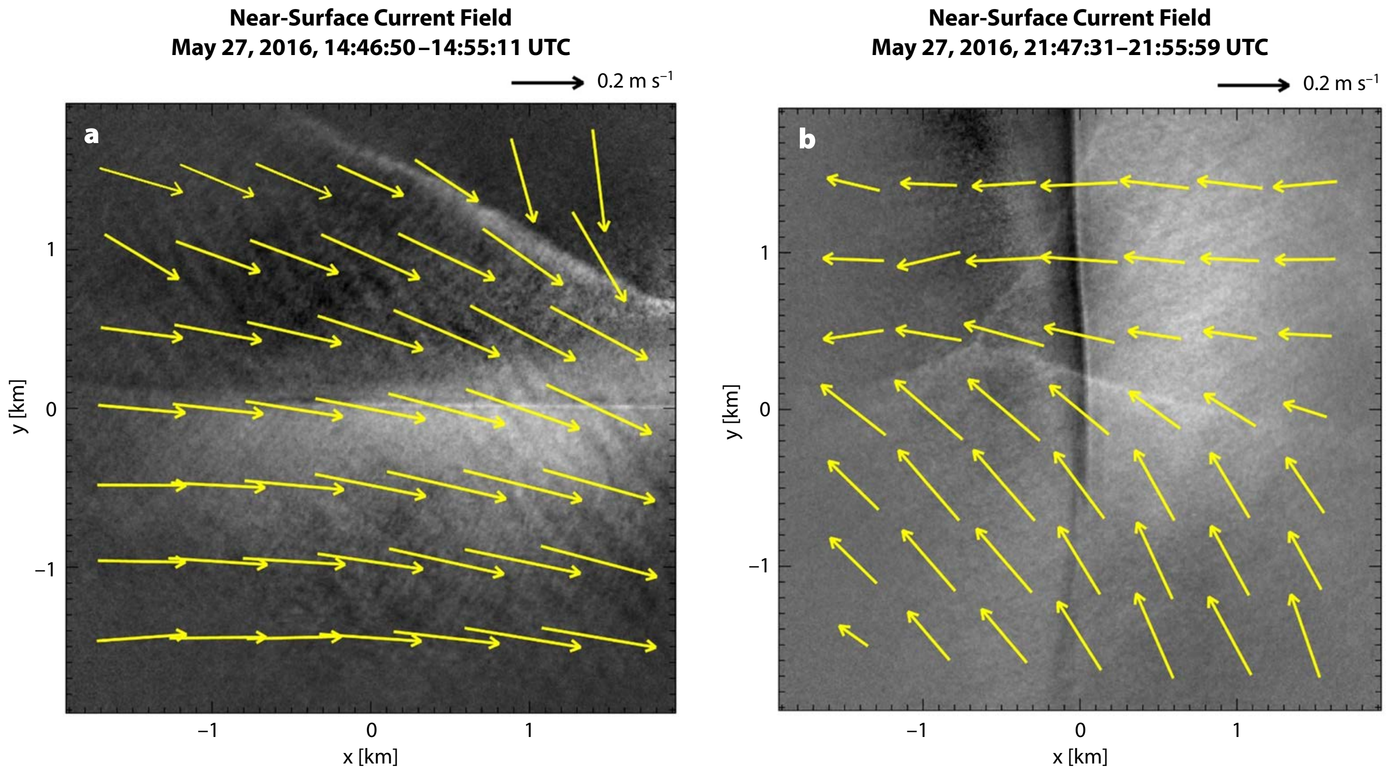

FIGURE 12. Two-dimensional near-surface current fields over convergent front sightings.

rent fields (Figure 12). It is important to note that the ship wake is visible as a horizontal line in the middle of Figure 12a, where the front is visible in the upper-right corner. In Figure 12b, the ship wake is the vertical line through the middle of the image and the front is the Y-shaped bright feature. It is easy to see from these current fields that the directionality of the near-surface current abruptly changes at the frontal interface. Both of these convergent fronts are also associated with underwater topography changes; the front in Figure 12a occurs during a 1,900 m bathymetry change over 10 km horizontally, and the front in Figure 12b is associated with a 1,500 m bathymetry change over 8 km horizontally.

CONCLUSION

DMR, with its wide range, portability, and spatiotemporal capabilities, is an invaluable resource for imaging upper ocean dynamic features. When used in combination with the large-scale view provided by SAR images, it is possible to detect underwater features that correspond to abrupt topography gradients in both shallow and deep water. Analysis of DMR and SAR images ultimately enhances vessel safety in these dynamic regions.

With the aid of these instruments, internal wave generation points can be determined using ray tracing. Two particular generation points were found in the region surrounding Palau: north of Velasco Reef as the flow is directed around the sunken atoll as well as over the southern tip of the Kyushu-Palau Ridge, and in the narrow passageways into open ocean between the islands of Kayangel and Babeldaob.

Collection of DMR images enabled identification of convergent fronts. Through advanced processing of multiple DMR rotations, this instrument can be used to measure near-surface currents by employing the dispersion shell method or the empirical DoVeS algorithm. These current measurements show that the surface features are indicative of near-surface current variations as a result of a large underwater topography change over a relatively small horizontal distance.

Identification of these upper ocean features helps us to further understand flow changes over steep underwater topography. Sighting of a frontal feature on a ship-mounted DMR provides an alert that there are converging surface currents at the location of the signature and therefore there may be an abrupt underwater topography change nearby. The examples provided in this paper indicate that abrupt shallow and deepwater bathymetry changes manifest as recognizable surface signatures in radar imagery.

REFERENCES

Alpers, W., and I. Hennings. 1984. A theory of the imaging mechanism of underwater bottom topography by real and synthetic aperture radar. *Journal of Geophysical Research* 89(C6):10,529–10,546, https://doi.org/10.1029/JC089iC06p10529.

Alpers, W. 1985. Theory of radar imaging of internal waves. *Nature* 314(6008):245–247, https://doi.org/10.1038/314245a0.

Alpers, W., G. Campbell, H. Wensink, and Q. Zhang. 2004. Underwater topography. Pp. 245–262 in *Synthetic Aperture Radar: Marine User's Manual*, C.R. Jackson and J.R. Apel, eds, US Department of Commerce, National Oceanic and Atmospheric

Administration, National Environmental Satellite, Data, and Information Serve, Office of Research and Applications.
Braun, N., F. Ziemer, A. Bezuglov, M. Cysewski, and G. Schymura. 2008. Sea-surface current features observed by Doppler radar. *IEEE Transactions on Geoscience and Remote Sensing* 46(4):1,125–1,133, https://doi.org/10.1109/TGRS.2007.910221.
Carrasco, R., J. Horstmann, and J. Seemann. 2017. Significant wave height measured by coherent X-band radar. *IEEE Transactions on Geoscience and Remote Sensing* 55(9):5,355–5,365, https://doi.org/10.1109/TGRS.2017.2706067.
Colin, P.L. 2009. *Marine Environments of Palau*. Indo-Pacific Press, 416 pp.
da Silva, J.C.B., S.A. Ermakov, I.S. Robinson, D.R.G. Jeans, and S.V. Kijashko. 1998. Role of surface films in ERS SAR signatures of internal waves on the shelf: Part 1. Short-period internal waves. *Journal of Geophysical Research* 103(C4)8,009–8,031, https://doi.org/10.1029/97JC02725.
Gade, M., V. Byfield, S. Ermakov, O. Lavrova, and L. Mitnik. 2013. Slicks as indicators for marine processes. *Oceanography* 26(2)138–149, https://doi.org/10.5670/oceanog.2013.39.
Hovland, H.A., J.A. Johannessen, and G. Digranes. 1994. Slick detection in SAR images. Pp. 2,038–2,040 in *Proceedings of IGARSS '94, 1994 IEEE International Geoscience and Remote Sensing Symposium,* https://doi.org/10.1109/IGARSS.1994.399647.
Hühnerfuss, H., and W. Alpers. 1983. Molecular aspects of the system water/monomolecular surface film and the occurrence of a new anomalous dispersion regime at 1.43 GHz. *The Journal of Physical Chemistry* 87(25):5,251–5,258, https://doi.org/10.1021/j150643a039.
Kobayashi, K. 2004. Origin of the Palau and Yap trench-arc systems. *Geophysical Journal International* 157(3):1,303–1,315, https://doi.org/10.1111/j.1365-246X.2003.02244.x.
Lamb, K.G. 1994. Numerical experiments of internal wave generation by strong tidal flow across a finite amplitude bank edge. *Journal of Geophysical Research* 99(C1)843–864, https://doi.org/10.1029/93JC02514.
Lund, B., H.C. Graber, K. Hessner, and N.J. Williams. 2015a. On shipboard marine X-band radar near-surface current "calibration." *Journal of Atmospheric and Oceanic Technology* 32(10)1,928–1,944, https://doi.org/10.1175/JTECH-D-14-00175.1.
Lund, B., H.C. Graber, H. Tamura, C. Collins III, and S. Varlamov. 2015b. A new technique for the retrieval of near-surface vertical current shear from marine X-band radar images. *Journal of Geophysical Research* 120(12):8,466–8,486, https://doi.org/10.1002/2015JC010961.
Lund, B., B.K. Haus, J. Horstmann, H.C. Graber, R. Carrasco, N.J. Laxague, G. Novelli, C.M. Guigand, and T.M. Özgökmen. 2018. Near-surface current mapping by shipboard marine X-band radar: A validation. *Journal of Atmospheric and Oceanic Technology* 35(5):1,077–1,090, https://doi.org/10.1175/JTECH-D-17-0154.1.
Lyzenga, D.R. 1991. Interaction of short surface and electromagnetic waves with ocean fronts. *Journal of Geophysical Research* 96(C6):10,765–10,772, https://doi.org/10.1029/91JC00900.
Nyman, L., B. Lund, R. Romeiser, H. Graber, and J. Horstmann. 2019. A new empirical approach to detect surface currents using Doppler marine radar. In *Proceedings of the 2019 IEEE/OES Twelfth Current, Waves, Turbulence Measurement and Applications (CWTMA)*, IEEE.
Senet, C.M., J. Seemann, and F. Ziemer. 2001. The near-surface current velocity determined from image sequences of the sea surface. *IEEE Transactions on Geoscience and Remote Sensing* 39(3)492–505, https://doi.org/10.1109/36.911108.
Valenzuela, G.R. 1978. Theories for the interaction of electromagnetic and oceanic waves: A review. *Boundary-Layer Meteorology* 13(1–4):61–85, https://doi.org/10.1007/BF00913863.
Wolanski, E., P. Colin, J. Naithani, E. Deleersnijder, and Y. Golbuu. 2004. Large amplitude, leaky, island-generated, internal waves around Palau, Micronesia. *Estuarine, Coastal and Shelf Science* 60(4)705–716, https://doi.org/10.1016/j.ecss.2004.03.009.
Wright, J. 1968. A new model for sea clutter. *IEEE Transactions on Antennas and Propagation* 16(2)217–223, https://doi.org/10.1109/TAP.1968.1139147.
Young, I.R., W. Rosenthal, and F. Ziemer. 1985. A three-dimensional analysis of marine radar images for the determination of ocean wave directionality and surface currents. *Journal of Geophysical Research: Oceans* 90(C1):1,049–1,059, https://doi.org/10.1029/JC090iC01p01049.

ACKNOWLEDGMENTS

COSMO-SkyMed™ Product-ASI 2016 processed under license from ASI (Agenzia Spaziale Italiana); all rights reserved. COSMO-SkyMed images were distributed by e-GEOS. TerraSAR-X data were obtained through © DLR e.V. 2016. TerraSAR-X images were distributed by Airbus Defense and Space GmbH; downlinked and processed by CSTARS under Airbus Defense and Space license. Lisa Nyman was funded by the US Office of Naval Research (ONR) under grants N00014-14-1-0630 and N00014-16-1-3147. We thank Samantha Ballard for assisting in the DMR installation on R/V *Roger Revelle.*

AUTHORS

Lisa Nyman (lnyman@rsmas.miami.edu) is PhD Candidate, **Björn Lund** is Associate Scientist, **Hans C. Graber** is Professor, and **Roland Romeiser** is Professor, all at the University of Miami Rosenstiel School of Marine and Atmospheric Science, Miami, FL, USA. **Jochen Horstmann** is Head, Department of Radar Hydrography, Helmholtz-Zentrum Geesthacht, Geesthacht, Germany.

ARTICLE CITATION

Nyman, L., B. Lund, H.C. Graber, R. Romeiser, and J. Horstmann. 2019. Radar observations of ocean surface features resulting from underwater topography changes. *Oceanography* 32(4):174–183, https://doi.org/10.5670/oceanog.2019.423.

COPYRIGHT & USAGE

This is an open access article made available under the terms of the Creative Commons Attribution 4.0 International License (https://creativecommons.org/licenses/by/4.0/), which permits use, sharing, adaptation, distribution, and reproduction in any medium or format as long as users cite the materials appropriately, provide a link to the Creative Commons license, and indicate the changes that were made to the original content.